Femtosecond spectroscopy of condensed phases with chirped supercontinuum probing

S. A. Kovalenko,* A. L. Dobryakov,† J. Ruthmann,‡ and N. P. Ernsting§
Institut für Physikalische und Theoretische Chemie, Humboldt Universität, D-10117 Berlin, Germany
(Received 25 June 1998)

Pump–*supercontinuum*-probe (PSCP) spectroscopy with femtosecond time resolution is developed theoretically and experimentally. The connection to previous theoretical results on nonchirped probing is established. It is experimentally shown that the supercontinuum can be described as a single chirped pulse. A key problem of the technique—the precise time correction of transient spectra—is solved by monitoring the nonresonant electronic response from a pure solvent (liquids) or from a transparent substrate (solid films). This allows for an adequate characterization of the supercontinuum, in particular, for directly measuring the spectral dependence of the pump-probe cross correlation. For 50-fs pump pulses, a theoretical estimate gives an accuracy for the time correction of 10 fs, which is typically ≈1/30 of the supercontinuum pulse duration. Hence a time resolution of 10–20 fs can be experimentally realized. Contributions to the nonresonant transient signal from high-frequency Raman excitations and from low-frequency impulsive-stimulated Raman processes are discussed. The PSCP technique is illustrated by results from experiments with fused silica and several common solvents and with a chromophore in solution. [S1050-2947(99)03303-X]

PACS number(s): 42.65.Re, 42.65.−k

I. INTRODUCTION

Broadband femtosecond pump-probe spectroscopy with Fourier transform-limited pulses has been developed experimentally [1–4] and theoretically [2,5–11] during the last decade and shown to be a powerful tool for studying ultrafast processes in molecules and their environment. Currently available 5–10-fs pulses provide a spectral width of more than 1000 cm^{-1}, which, however, is still not enough to characterize, for example, transient spectra of polar chromophors in dipolar liquids. In the condensed phase, vibronic transitions are broadened considerably by interaction with the environment. Monitoring the ultrafast evolution requires broad spectral coverage (typically of 10 000 cm^{-1}) in order to expose spectral structure as well as its ultrafast diffusion and drift. A natural way to satisfy this condition, while preserving high time resolution, is to apply a supercontinuum [12–14] (SC) as a probe. Recently this pump–supercontinuum-probe (PSCP) spectroscopy has proved its efficiency for monitoring femtosecond response in both liquids [15–27] and solids [28,29]. But the use of supercontinuum probing poses the question as to what extent theories [2,5–11] developed for transform-limited nonchirped (NC) probe pulses are applicable for the PSCP spectroscopy.

It is well known that the supercontinuum is chirped due to self-phase modulation and group velocity dispersion in the material in which it is generated. Hence different spectral components of the probe enter the sample at different times for any specific setting of the pump-probe delay. In an intuitive approach, which is usually taken implicitly, the supercontinuum is represented as a single chirped pulse, with spectral components which interact with the pump independently and do not influence each other. This implies that the time-corrected PSCP signal can be described by the theories developed for NC probe pulses. However, this approach, its limits, and consequences have not been rigorously discussed yet, although the femtosecond PSCP technique may be considered to have started [12] in 1982. This lack of a theoretical basis forced some workers either to measure only at fixed wavelengths [17,20,26], which is time consuming and leads to a loss of spectral resolution (because the signal is usually measured with 10–20-nm steps), or to avoid the region of pump-probe pulse overlap [15,18], which deteriorates the time resolution. Note that the SC pulse duration is typically hundreds of fs, while the pump pulse can be adjusted to a few tens of fs. Hence, with a proper treatment of a PSCP experiment, one can expect an order of magnitude improvement for the time resolution.

A further important problem concerns the time correction procedure itself. In general, it may be performed by replacing the investigated medium with a nonlinear crystal and measuring the upconverted signal for different probe wavelengths [14]. However, in practice, this is not convenient and may introduce errors. As has been shown by us earlier [21], there is a more direct and precise method for time correction by monitoring the nonresonant coherent signal either from pure solvents (liquids) or from a transparent substrate (solid films). A considerable advantage for resonant measurements, in addition to the adequate characterization of the supercontinuum, is that the nonresonant contribution can be subtracted [25] from the total signal to obtain the true transient absorption spectra by the medium under study. This subtraction is of particular importance for overlapped pump and probe pulses to obtain the resonant coherence effects only. These effects have been extensively studied before both for nonchirped [30–34] and chirped pulses [32,35–37], but in the degenerate case, when the pump and probe are derived

*On leave from the Institute of Chemical Physics, Russian Academy of Sciences, Moscow 117977, Russian Federation
†Present address: Institute of Spectroscopy, Russian Academy of Sciences, Troitsk, Moscow Region 142092, Russia
‡Present address: Institut für Chemo- und Biosensorik, Mendelstr. 7, D-48149 Münster, Germany.
§Electronic address: nernst@npe01.chemie.hu-berlin.de

from the same source. They have been also discussed for different pump and probe frequencies [2,5,6,8,15,38–40], but for NC pulses. For our experimental conditions (chirped probe and NC pump pulses), we discuss these contributions only briefly. Instead, we concentrate on the nonresonant signal, in which case an analytical expression for the transient signal can be obtained and comparison with experimental results is straightforward.

Among previous studies with SC probing, the linear chirp representation was first introduced by Walkup *et al.* [41] to treat a gas phase experiment with dissociating molecules. They did not explicitly use the time correction procedure, but calculated the transient signal directly. Later Tokunaga *et al.* [42] characterized the supercontinuum as a single nonlinearly chirped pulse and discussed the time correction for their specific transient phase and transmission spectroscopy with interferometric configuration. This treatment is close in spirit to our approach.

In the present article we establish the theoretical and experimental background of the PSCP technique. A theory of measurements with SC probing is presented in Sec. II, where the supercontinuum is treated as a single chirped pulse [21,41,42]. We show that for a general but ''slow'' response function $R(t)$ the simulated transient signal, after time correction, is identical to that calculated for NC probe pulses, in agreement with the intuitive approach. The difference between two types of probing becomes prominent when $R(t)$ is fast and resembles a $\delta(t)$ response. The validity of our treatment is tested in Sec. III, where our simulations are compared to experimental results obtained for nonresonant (fused silica, pure solvents) and resonant excitation (a chromophore in solution). We summarize the results in Sec. IV. A preliminary treatment of some questions discussed in this article was already given in Ref. [21].

II. THEORETICAL

A. Background

In a pump-probe experiment, the electric field $E(\mathbf{r},t)$ in the sample is given by

$$E(\mathbf{r},t)=E_1(t)\exp(-i\mathbf{k}_1\cdot\mathbf{r})+E_2(t-t_d)\exp(-i\mathbf{k}_2\cdot\mathbf{r})+\text{c.c.}, \tag{1}$$

where $E_1(t)$ and $E_2(t)$ are the pump and probe field with a wave vector $\mathbf{k}_1$ and $\mathbf{k}_2$, respectively, t_d is the pump-probe delay, and c.c. stands for complex conjugate. Throughout the article we consider the sample as a thin optical medium and therefore neglect propagation effects. The differential optical signal $\Delta D(\omega_2,t_d)$ induced by pumping can be written as [2,6,8,10]

$$\Delta D(\omega_2,t_d)=-2\omega_2\,\mathrm{Im}[E_2^*(\omega_2)P^{(3)}(\omega_2,t_d)]/|E_2(\omega_2)|^2. \tag{2}$$

Here $P^{(3)}(\omega_2,t_d)$ is the third-order polarization, and we introduced the Fourier transform $\mathcal{T}$ of a function $f(t)$ as

$$f(\omega)=\mathcal{T}(f(t))=\int_{-\infty}^{\infty}dt\,f(t)\exp(-i\omega t), \tag{3a}$$

$$E_2(\omega_2)=\int_{-\infty}^{\infty}dt\,E_2(t)\exp(-i\omega_2 t), \tag{3b}$$

$$P^{(3)}(\omega_2,t_d)=\int_{-\infty}^{\infty}dt\,P^{(3)}(\mathbf{k}_2,t,t_d)\exp(-i\omega_2 t). \tag{3c}$$

Equation (2) is written under the condition $|P^{(3)}(\omega_2)| \ll |E_2(\omega_2)|$. In this case, $E_2(\omega_2)$ plays the role of a local oscillator field and the signal $\Delta D(\omega_2,t_d)$ is linearly dependent on $P^{(3)}(\omega_2,t_d)$. Linearity is an important feature of the pump-probe technique because it allows the subtraction of different contributions (e.g., from the solvent) to $P^{(3)}(\omega_2,t_d)$ if they are known or can be measured independently.

Further, we adopt the treatment of nonlinear spectroscopy developed by Mukamel and co-workers [6,8,40]. Consider a molecular system with a ground state $|g\rangle$ and excited electronic states $|e\rangle$ and $|f\rangle$, in which case the molecular Hamiltonian is [6,40] $H=|g\rangle H_g\langle g|+|e\rangle H_e\langle e|+|f\rangle H_f\langle f|$. When necessary, each electronic state can be expanded into vibronic eigenstates denoted as $|\alpha\rangle$, $|\beta\rangle$, and $|\gamma\rangle$, respectively. To keep notation simple, we do not use this expansion explicitly. The pump pulse is in resonance with the $g\rightarrow e$ transition: the probe covers both the $g\leftrightarrow e$ transitions and $e\rightarrow f$ excited-state absorption. The nonlinear polarization $P^{(3)}(\mathbf{k}_2,t,t_d)$ is given by [6]

$$\begin{aligned}P^{(3)}(\mathbf{k}_2,t,t_d)=&\int_0^{\infty}dt_3\int_0^{\infty}dt_2\int_0^{\infty}dt_1\\&\times\mathcal{R}^{(3)}(t_3,t_2,t_1)E(\mathbf{r},t-t_3-t_2-t_1)\\&\times E(\mathbf{r},t-t_3-t_2)E(\mathbf{r},t-t_3)\end{aligned} \tag{4a}$$

where $\mathcal{R}^{(3)}(t_3,t_2,t_1)$ is the third-order nonlinear response function which is written as

$$\mathcal{R}^{(3)}(t_3,t_2,t_1)=i\sum_{\alpha=1}^{4}[S_\alpha(t_3,t_2,t_1)-S_\alpha^*(t_3,t_2,t_1)], \tag{4b}$$

$$\begin{aligned}S_1(t_3,t_2,t_1)=&\sum_{v=f,g}|\mu_{ve}|^2|\mu_{eg}|^2\\&\times\langle G_{ve}(t_3)G_{ee}(t_2)G_{ge}(t_1)\rho_g\rangle,\end{aligned}$$

$$\begin{aligned}S_2(t_3,t_2,t_1)=&\sum_{v=f,g}|\mu_{ve}|^2|\mu_{eg}|^2\\&\times\langle G_{ve}(t_3)G_{ee}(t_2)G_{eg}(t_1)\rho_g\rangle,\end{aligned}$$

$$\begin{aligned}S_3(t_3,t_2,t_1)=&\sum_{v=f,g}|\mu_{ve}|^2|\mu_{eg}|^2\\&\times\langle G_{ve}(t_3)G_{vg}(t_2)G_{eg}(t_1)\rho_g\rangle,\end{aligned}$$

$$\begin{aligned}S_4(t_3,t_2,t_1)=&\sum_{v=f,g}|\mu_{ve}|^2|\mu_{eg}|^2\\&\times\langle G_{ge}(t_3)G_{gv}(t_2)G_{ge}(t_1)\rho_g\rangle.\end{aligned} \tag{4c}$$

Here μ_{nm} designates the optical transition dipole moment, ρ_g is the initial equilibrium density matrix in the ground state, and $v=g,f$. The Green's functions $G_{nm}(t)$ are defined by its action on a nuclear operator A as $G_{nm}(t)A \equiv \exp(-iH_n t)A\exp(iH_m(t))$. The asterisk $(*)$ means the complex conjugate, and $\langle\cdots\rangle$ denotes averaging over nuclear degrees of freedom.

As is seen from Eqs. (4a)–(4c), the system is always in electronic coherence ρ_{ge} or ρ_{eg} during the t_1 period and in electronic coherence ρ_{ev} or ρ_{ve} during the t_3 period. During the t_2 interval, it may be in electronic population state ρ_{gg} or ρ_{ee} as well as in coherence ρ_{gf} or ρ_{fg}. Each term S_α or S_α^*, when combined with the properly ordered pump and probe field, corresponds to a particular evolution of the system, starting from the ground state ρ_g. When the system interacts first twice with the pump and then with the probe, this results in the so-called sequential contributions to the transient signal. If the order of interactions is mixed (pump-probe-pump or probe-pump-pump), then the coherent, Raman, and two-photon absorption contributions appear. The coherent terms exist only for overlapped pump and probe pulses, while sequential terms contribute also for well-separated pulses.

Another important difference between the three contributions becomes clear when considering the evolution during the t_2 period. For the sequential terms, the system is always in a population state $\rho_{\alpha\alpha}$ or $\rho_{\beta\beta}$ (we neglect for the moment an impulsive Raman excitation), and its evolution is governed by population relaxation and spectral diffusion processes. In contrast the Raman terms correspond to vibrational coherences [6,15,39] $\rho_{\alpha\alpha'}$ and $\rho_{\beta\beta'}$, and their evolution is governed by *vibrational dephasing*. In the degenerate case, when the pump and probe frequency are identical, these terms are known as transient grating contributions [30–34]. Last, the two-photon absorption terms correspond to electronic coherences $\rho_{\alpha\gamma}$ and $\rho_{\gamma\alpha}$ and are governed by *electronic dephasing* during the t_2 period. A typical time scale for electronic dephasing at room temperature is $\sim$10 fs, while for vibrational dephasing it is often slower than 1 ps. Therefore the coherent two-photon absorption terms are usually much smaller than the Raman contributions.

In the following we assume that the laser pulses are long compared to electronic dephasing [6,40,43]. In this case the triple integration Eq. (4a) can be reduced to a single one, and calculations of the transient signal are greatly simplified. This approach is sufficient for a comparison between SC and NC probing when one considers only population relaxation in the excited state of the sample. A triple integration is necessary in the general case, when evaluating the relative contributions from coherent and sequential terms to the resonant signal [15,34,40]. This problem will not be discussed in this article. Then, by substituting Eq. (1) in Eq. (4a), we obtain, in the rotating-wave approximation and at condition $\mathbf{k}_2=-\mathbf{k}_1+\mathbf{k}_1+\mathbf{k}_2$,

$$\begin{aligned}P^{(3)}(\mathbf{k}_2,t,t_d)=&2E_2(t-t_d)\int_{-\infty}^{\infty}dt' R_S(t-t')\\&\times E_1^*(t')E_1(t')+2E_1(t)\int_{-\infty}^{\infty}dt'\\&\times R_R(t-t')E_1^*(t')E_2(t'-t_d)\\&+2E_1^*(t)\int_{-\infty}^{\infty}dt' R_{2ph}(t-t')\\&\times E_1(t')E_2(t'-t_d).\end{aligned}\tag{5}$$

The three terms correspond to the sequential, Raman, and two-photon absorption contributions with their reduced response functions R_S, R_R, and $R_{2\mathrm{ph}}$, respectively. Remember that the response functions are zero for negative arguments. The different structure of the three contributions is best seen for NC probe pulses, in which case Eq. (5) becomes [44]

$$\begin{aligned}P^{(3)}(\mathbf{k}_2,t,t_d)=&2\exp[i\Omega_2(t-t_d)]\\&\times\Bigg\{\varepsilon_2(t-t_d)\int_{-\infty}^{\infty}dt' R_S(t-t')\varepsilon_1^*(t')\varepsilon_1(t')\\&+\varepsilon_1(t)\int_{-\infty}^{\infty}dt' R_R(t-t')\varepsilon_1^*(t')\\&\times\varepsilon_2(t'-t_d)\exp[i(\Omega_1-\Omega_2)(t-t')]+\varepsilon_1^*(t)\\&\times\int_{-\infty}^{\infty}dt' R_{2\mathrm{ph}}(t-t')\varepsilon_1(t')\varepsilon_2(t'-t_d)\\&\times\exp[-i(\Omega_1+\Omega_2)(t-t')]\Bigg\}+\text{c.c.},\end{aligned}\tag{6}$$

where ε_1, ε_2 and Ω_1, Ω_2 are the slowly varying amplitude and central frequency of the pump and probe pulses, respectively. We see directly that the last two terms contribute only when the response function has resonances at frequencies $\Omega_1\mp\Omega_2$. As discussed above, the two-photon absorption term is small compared to the Raman contribution due to ultrafast electronic dephasing. We drop this term in the resonance case, but it must be taken into account for calculations of the pure nonresonant electronic contribution (see Sec. II C).

B. Supercontinuum versus nonchirped probing

We assume that the pump pulse is a nonchirped Gaussian

$$E_1(t)=a_1\exp[-t^2/2\tau_1^2+i\Omega_1 t],\tag{7}$$

with amplitude a_1 and duration τ_1. The supercontinuum probe is generally represented by a pulse with an arbitrary chirp. First, we discuss the simple case of linear chirp:

$$E_2(t)=\exp[-t^2/2\tau_2^2+i(\Omega_2 t+\beta t^2)],\tag{8a}$$

$$E_2(\omega_2)=\tau_2\sqrt{2\pi/\alpha}\exp[-\tau_2^2(\omega_2-\Omega_2)^2/2\alpha].\tag{8b}$$

Here Ω_2, τ_2, and β are the central frequency, pulse duration, and chirp rate, respectively, and $\alpha=1-i2\beta\tau_2^2$. An intuitive treatment of the PSCP experiment is the following. The probe pulse has an instantaneous frequency $\Omega_2(t)=\Omega_2+2\beta t$, which is now time dependent. Hence different spectral components of the supercontinuum interact with the pump at different delays. Therefore we introduce the so-called time-zero function $t_0(\omega_2)$ as

$$t_0(\omega_2)\approx(\omega_2-\Omega_2)/2\beta.\tag{9}$$

Equation (9) defines the actual delay between the pump and the ω_2 spectral component of the probe, provided t_d has been set to zero at $\omega_2=\Omega_2$. For positive chirp $\beta>0$, the blue components of the probe follow the red ones, in agreement with experimental observations. For arbitrary chirp, Eq. (8b) for the SC field can be written as $E_2(\omega_2)=|E_2(\omega_2)|\exp[i\Phi(\omega_2)]$; then, Eq. (9) is generalized to

$$t_0(\omega_2)=-\partial\Phi/\partial\omega_2\equiv-\Phi'(\omega_2), \tag{10}$$

where $\Phi(\omega_2)$ is the phase of the supercontinuum. Equation (10) reduces to Eq. (9) for a linear chirp at condition $2\beta\tau_2^2\gg1$, which is usually the case and therefore assumed for the rest of the article. Then the total frequency-dependent pump-probe delay $t_d(\omega_2)$ becomes

$$t_d(\omega_2)=t_d+t_0(\omega_2). \tag{11}$$

When the time-zero function $t_0(\omega_2)$ is known, the experimental transient spectra can be time corrected and the true response functions $R_{S,R}(t)$ can be obtained. Let us now consider how this approach may be justified in a rigorous way.

First, we calculate the differential signal $\Delta D(\omega_2,t_d)$ by using Eqs. (2), (3), (5), and (7). After some rearrangements, integration in Eq. (5) results in

$$\Delta D(\omega_2,t_d)=-(2\omega_2|a_1|^2\tau_1/\sqrt{\pi})\mathrm{Im}(J_S+J_R), \tag{12a}$$

$$J_S=\int_{-\infty}^{\infty}d\Omega E_2^*(\omega_2)E_2(\omega_2-\Omega)R_S(\Omega)\times\exp\left(-\frac{\tau_1^2\Omega^2}{4}+i\Omega t_d\right), \tag{12b}$$

$$J_R=(\tau_1/\sqrt{\pi})\int_{-\infty}^{\infty}d\Omega\int_{-\infty}^{\infty}d\Omega' E_2^*(\omega_2)\times E_2(\omega_2-\Omega')R_R(\Omega)\exp\left(-\frac{\tau_1^2}{2}[(\omega_2-\Omega_1-\Omega)^2+(\Omega+\Omega'-\omega_2+\Omega_1)^2]+i\Omega' t_d\right). \tag{12c}$$

In Eq. (12) and below, we put $|E_2(\omega_2)|=1$. The two contributions J_S and J_R correspond to the sequential and Raman terms in Eq. (5) and $R_{S,R}(\Omega)=\mathcal{T}(R_{S,R}(t))$.

Next, we model an arbitrary supercontinuum $E_2(\omega_2)$ by a Gaussian as $E_2(\omega_2)=E_2^c(\omega_2)\exp[i\Phi(\omega_2)]$. Here $E_2^c(\omega_2)=\exp[-\tau_c^2(\omega_2-\Omega_2)^2/2]$ is the amplitude of the SC with a spectral width of $1/\tau_c$ and $\Phi(\omega_2)$ is the phase. [An example of this approximation to an experimental supercontinuum is shown in Fig. 6(a); for a linear chirp, one has $\tau_c^2=\tau_2^2/|\alpha|^2$.] Using this representation and the expansion $\Phi(\omega_2-\Omega)\approx\Phi(\omega_2)-\Phi'(\omega_2)\Omega+\Phi''(\omega_2)\Omega^2/2$, we rewrite Eqs. (12b) and (12c) as

$$J_S=\int_{-\infty}^{\infty}d\Omega\, R_S(\Omega)\exp(-A\Omega^2+B\Omega), \tag{13a}$$

$$J_R=\sqrt{2/\delta}\exp(B^2/4A-B_1^2/4A_1)\times\int_{-\infty}^{\infty}d\Omega\, R_R(\Omega)\exp(-A_1\Omega^2+B_1\Omega), \tag{13b}$$

$$A=\tau_1^2/4+\tau_c^2/2-i\Phi''(\omega_2)/2, \tag{13c}$$

$$B=i[t_d-\Phi'(\omega_2)]+\tau_c^2(\omega_2-\Omega_2), \tag{13d}$$

where $A_1=2A/\delta$, $B_1=(4A(\omega_2-\Omega_1)-B)/\delta$, and $\delta=1+\tau_c^2/\tau_1^2-i\Phi''(\omega_2)/\tau_1^2$.

For population relaxation processes, an arbitrary response function can be expressed as $R_s(\Omega)=\Sigma a_j/(i\gamma_j-\Omega)$. Therefore we evaluate the differential signal $\Delta D(\omega_2,t_d)$ in the simplest case $R_s(\Omega)=1/(i\gamma-\Omega)$, where γ is the population decay rate constant. Similarly for Raman terms, the reduced response function is built from expressions $R_R^{(1,2)}(\Omega)=1/(i\gamma_n\pm\omega_n-\Omega)$, with decay rate constant γ_n for vibrational coherence at nuclear frequency ω_n. The integrals (13a) and (13b) are calculated with the relation

$$\int_{-\infty}^{\infty}d\Omega\frac{\exp(-A\Omega^2+B\Omega)}{\Omega-i\gamma}=i\pi\exp\left(\frac{B^2}{4A}\right)W(i\gamma\sqrt{A}-B/2\sqrt{A}). \tag{14}$$

Here $W(z)$ [45] is expressed through the error function $\mathrm{erfc}(-iz)$ of the complex argument z:

$$W(z)=(i/\pi)\int_{-\infty}^{\infty}dt[\exp(-t^2)]/(z-t)=\exp(-z^2)\mathrm{erfc}(-iz). \tag{15}$$

Thus the signal is determined by

$$J_S=-i\pi\exp(B^2/4A)W(i\gamma\sqrt{A}-B/2\sqrt{A}), \tag{16a}$$

$$J_R^{(1,2)}=-i\pi\sqrt{2/\delta}\exp(B^2/4A)\times W(i\gamma_n\sqrt{A_1}-B_1/2\sqrt{A_1}\pm\omega_n\sqrt{A_1}). \tag{16b}$$

Note that the Raman term J_R vanishes when $[t_d+t_0(\omega_2)]\gg\tau_1$. In this case $W(z)\sim\exp(-z^2)$, and Eq. (16b) gives $J_R\sim\exp\{-[t_d+t_0(\omega_2)]^2/2\tau_1^2\}\to0$. In the remainder of this section, we discuss only the first, sequential term in Eq. (5) or (12a). We evaluate now the sequential contribution J_s to the resonant signal, at the above condition of nonoverlapped pump and probe pulses, for two limiting cases.

For *nonchirped probe pulses*, $\Phi'(\omega_2)=\Phi''(\omega_2)=0$, $E_2(\omega_2)=\exp[-\tau_2^2(\omega_2-\Omega_2)^2/2]$, $A=\tau_1^2/4+\tau_2^2/2$, and $B=it_d+\tau_2^2(\omega_2-\Omega_2)$. When $\tau_2\ll\tau_1$, one obtains, from Eqs. (12a) and (16a),

$$\Delta D(\omega_2,t_d)\propto\exp(-\gamma t_d+\gamma^2\tau_1^2/4)\mathrm{erfc}(\gamma\tau_1/2-t_d/\tau_1)=\int_{-\infty}^{\infty}dt' R_S(t')F_{cc}(t_d-t'), \tag{17}$$

where $F_{cc}(t)=\exp(-t^2/\tau_1^2)$ is the pump-probe cross correlation. The last equality in Eq. (17) represents the well-known

relation for the sequential contribution to the pump-probe signal, which is written here for an arbitrary response function $R_S(t)$.

In case of *chirped probe pulses*, one obtains

$$\Delta D(\omega_2,t_d)=2\sqrt{\pi}\omega_2|a_1|^2\tau_1\{\mathrm{Re}[2\exp(\gamma^2A+i\gamma B) -\exp(B^2/4A)W(B/2\sqrt{A}-i\gamma\sqrt{A})]\}. \quad (18)$$

For delay times $(t_d+t_0(\omega_2))\gg\tau_1$, the second term can be neglected and the differential signal, as given by the sequential term, becomes

$$\Delta D(\omega_2,t_d)\propto\mathrm{Re}[\exp(\gamma^2A+i\gamma B)] \approx\mathrm{Re}(2\exp\{-\gamma[t_d+t_0(\omega_2)] +(\gamma^2\tau_1^2/4)[1-2i\Phi''(\omega_2)/\tau_1^2]\}). \quad (19)$$

The second term in Eq. (18) contributes when $t_d(\omega_2)<\tau_1$. For this time interval the signal is given by

$$\Delta D(\omega_2,t_d)=\mathrm{Re}[\exp(B^2/4A)W(i\gamma\sqrt{A}-B/2\sqrt{A})] \approx\exp\{-[t_d+t_0(\omega_2)]^2/\tau_1^2\}. \quad (20)$$

As follows from Eqs. (19) and (20), the difference between nonchirped and chirped probing consists in a temporal shift (time correction) $t_d\to t_d+t_0(\omega_2)$ and an amplitude correction factor $(1-\gamma^4/32\beta^2)$ which derives from the imaginary part of the argument in Eq. (19). Typically $\beta\approx10^{-3}\,\mathrm{fs}^{-2}$, which leads to a small correction to the signal when $\gamma<(1/20)\,\mathrm{fs}^{-1}$. This is illustrated in Fig. 1 where the transient signal, simulated with a linearly chirped probe pulse (circles), is compared to that obtained with a nonchirped probe pulse (solid line). The two signals are indistinguishable for a wide range of γ.

Supposing that the above estimate is fulfilled, we can rewrite Eq. (18) in a form which is similar to Eq. (17):

$$\Delta D(\omega_2,t_d)=\int_{-\infty}^{\infty}dt'R_S(t')F_{\mathrm{cc}}(t_d+t_0(\omega_2)-t'). \quad (21)$$

Equation (21) constitutes the main result of this subsection. It confirms that the time-corrected transient signal, when measured with chirped probe pulses, is given by the same expression as that obtained with NC pulses. It was derived for a simple response function, but should be valid in general too.

Further below we show that the time-zero function $t_0(\omega_2)$ can be experimentally obtained from the femtosecond response of fused silica, which contains mainly the instantaneous electronic contribution. We shall also discuss other contributions to the nonresonant PSCP signal. In the nonresonant case, Eq. (5) is valid exactly and the response function $R(t)$ can be specified. Therefore the theoretical results of the following subsection should provide a sensitive test for the assumption, made above, that the SC probe can be represented as a single nonlinearly chirped pulse.

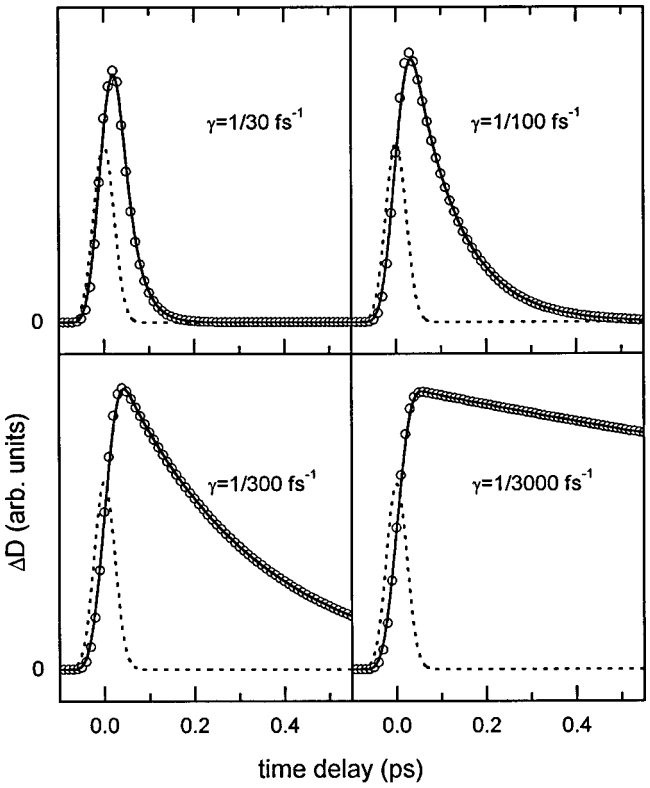

FIG. 1. Resonance transient signal at a fixed wavelength for a simple response function $R_S(\Omega)=1/(i\gamma-\Omega)$ simulated for linearly chirped SC probing after time correction [circles, using Eq. (18)] and for NC probe pulses (solid line). Parameters γ are given as insets. The other parameters are the same as in Fig. 2. The pump-probe cross correlation is shown by a dotted line.

C. Nonresonant PSCP spectroscopy

In the nonresonant case, the transient signal can be calculated directly from Eqs. (2) and (5) with the response functions $R_{S,R}$ given by [44,46,47]

$$R_{S,R}(t)\equiv R(t)=\sigma_e\delta(t)+\sigma_n\exp(-\gamma_nt)\sin(\omega_nt), \quad t\geqslant0. \quad (22)$$

Here the first term is the instantaneous electronic response with amplitude σ_e. The second term represents high- ($\omega_R\equiv\omega_n\gg1/\tau_1$) or low- ($\omega_n\leqslant1/\tau_1$) frequency nuclear vibrations with vibrational dephasing rate constant γ_n in the ground state of the sample. They correspond either to solvent vibrations (intra- and intermolecular) or to phonons in solids. To be specific, assume a pump pulse duration of $\tau_1=50\,\mathrm{fs}$. Then the characteristic wave numbers for low- and high-frequency modes will be 100 and 1000 cm^{-1}, respectively. The difference between the two types of excitations is that the high-frequency modes contribute only at fixed probe frequencies $\omega_2=\Omega_1\pm\omega_n$, while the low-frequency modes, as well as the coherent electronic part, give a transient signal over the whole spectral range of probing. Next, we discuss these contributions separately and compare the results for NC and SC probe pulses.

1. Coherent electronic contribution

For transparent media the electronic part of the transient signal is usually 5–6 times higher in magnitude than that

from low-frequency vibrations [48,49]. In addition, high-frequency modes may be weak, as in the case of fused silica. This material is widely used as windows or substrates in many femtosecond experiments. Therefore its transient response, which contains mainly the instantaneous electronic contribution, is of particular importance. In this case all three terms in Eq. (5) become equivalent.

We first discuss *linearly chirped probe pulses*. Using Eqs. (8b) and (12), we obtain an analytical expression for the electronic contribution ΔD_e:

$$\Delta D_e(\omega_2,t_d) = -6\omega_2|a_1|^2\sigma_e\tau_1\,\mathrm{Im}\{\sqrt{1/A}\,\exp[B^2/4A]\}, \tag{23a}$$

$$A = \tau_1^2/4 + \tau_2^2/2\alpha = \eta\tau_1^2/4, \tag{23b}$$

$$B = it_d + \tau_2^2(\omega_2-\Omega_2)/\alpha = i[t_d+t_0(\omega_2)] + t_0(\omega_2)/2\beta\tau_2^2, \tag{23c}$$

where $\alpha = 1 - i2\beta\tau_2^2$, $\eta = (1+2\xi^2/\alpha)$, and $\xi = \tau_2/\tau_1$. The second equality in Eq. (23c) relates parameter B to the time-zero function $t_0(\omega_2)$ defined in Eq. (10). Then the electronic signal can be written as

$$\Delta D_e(\omega_2,t_d) = -12\omega_2|a_1|^2\sigma_e/\sqrt{|\eta|} \times \mathrm{Im}\left\{\exp\left[-\frac{[t_d+t_0(\omega_2)]^2}{\eta\tau_1^2} + i\frac{t_0(\omega_2)}{\beta\tau_2^2}\frac{t_d+t_0(\omega_2)}{\eta\tau_1^2} + \left(\frac{t_0(\omega_2)}{2\beta\tau_2^2}\right)^2\frac{1}{\tau_1^2\eta} - i\varphi/2\right]\right\}, \tag{24}$$

where $\varphi = \arctan(\mathrm{Im}\,\eta/\mathrm{Re}\,\eta)$. For the practically important case when $2\beta\tau_2^2 \gg 1$, one has $|\eta| \approx 1$, $\varphi \approx 1/\beta\tau_1^2$, and the signal becomes

$$\Delta D_e \approx D_e^0 \exp\left[-\frac{[t_d+t_0(\omega_2)]^2}{\tau_1^2}\right] \times \sin\left[\frac{1}{2\beta\tau_1^2} - \frac{[t_d+t_0(\omega_2)]^2}{\beta\tau_1^4} - \frac{t_0(\omega_2)[t_d+t_0(\omega_2)]}{\beta\tau_2^2\tau_1^2}\right], \tag{25}$$

with $D_e^0 = 12\omega_2|a_1|^2\sigma_e/\sqrt{|\eta|}$. If in addition $\xi = \tau_2/\tau_1 \gg 1$, Eq. (25) simplifies to

$$\Delta D_e \approx D_e^0 \exp\{-[t_d+t_0(\omega_2)]^2/\tau_1^2\} \times \sin\{1/2\beta\tau_1^2 - [t_d+t_0(\omega_2)]^2/\beta\tau_1^4\}. \tag{26}$$

Expressions (25) and (26) must be compared with the frequency-dependent cross-correlation function $F_{cc}(\omega,t_d)$ between the pump and supercontinuum probe:

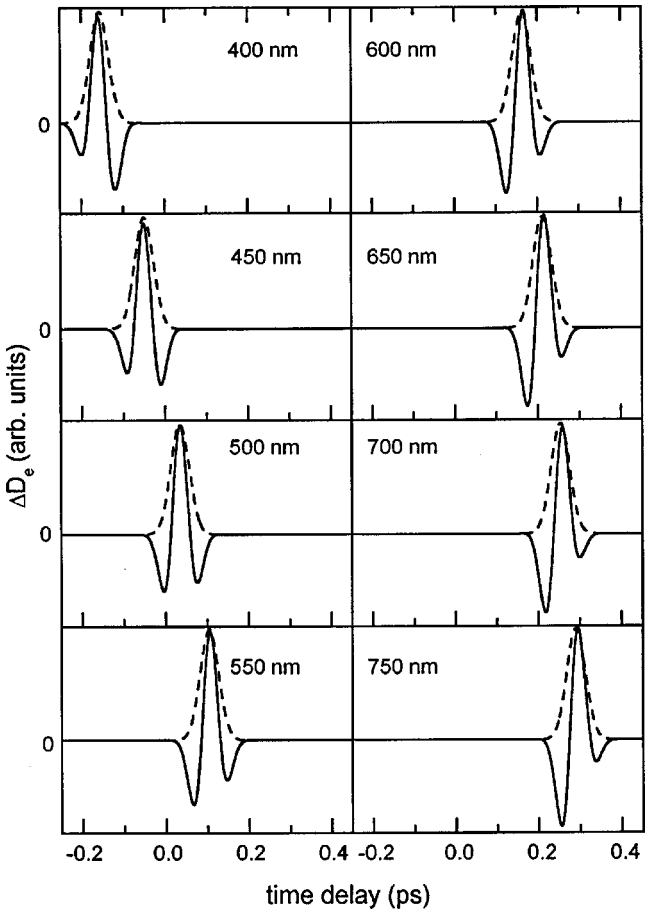

FIG. 2. Electronic signal $\Delta D_e(\omega_2,t_d)$ (solid line) calculated with Eq. (25) for linearly chirped SC probing: $\tau_1 = 50$ fs, $\xi = 4.4$, $\beta = 1.7\times10^{-3}$ fs^{-2}, $\beta\tau_1^2 = 2.2$, and $\beta\tau_2^2 = 42$. The pump-probe cross correlation F_{cc} as in Eq. (27) is shown by a dashed line. The pump pulse is centered at 480 nm. Probe wavelengths are given as insets.

$$F_{cc}(\omega_2,t_d) = \left|\int dt\,\exp(-i\omega_2 t)E_2(t)E_1(t-t_d)\right|^2 \approx \exp\{-[t_d+t_0(\omega_2)]^2/\tau_1^2\}. \tag{27}$$

Equation (27) describes an experiment [12] in which the field $E(\mathbf{k}) \propto E_1E_2$ is generated in a nonlinear crystal at sum frequency $\omega = \Omega_1 + \omega_2$ and for noncollinear geometry $\mathbf{k} = \mathbf{k}_1 + \mathbf{k}_2$, and then the spectrally dispersed signal is registered by a detector. The second equality is obtained at the above condition of a fast chirp rate $2\beta\tau_2^2 \gg 1$, in which case the cross-correlation width is equal to the pump pulse duration.

As is seen from Eqs. (25) and (26), the signal $\Delta D_e(\omega_2,t_d)$ reaches its positive maximum at $t_d = -t_0(\omega_2)$, that is, at the peak of the cross correlation. Thus the time-zero function $t_0(\omega_2)$ as well as the spectral phase $\Phi(\omega_2) \propto -\int d\omega_2 t_0(\omega_2)$ of the supercontinuum can be experimentally derived by measuring the electronic contribution to the transient signal.

Figure 2 shows the transient electronic signal $\Delta D_e(\omega_2,t_d)$ (solid lines) simulated for different probe wavelengths with Eq. (25). The parameters are close to those from the experimental section: $\tau_1 = 50$ fs, $\beta = 1.7\times10^{-3}$ fs^{-2}, $\beta\tau_2^2 = 40$, $\xi = 4.4$, and $\lambda_{pump} = 480$ nm. The electronic spike is seen to shift in time with the probe wavelength, as ex-

pected for chirped probing. The deviation of the maximum of the signal from true time zero, shown by the peak of the cross correlation $F_{cc}(\omega,t_d)$ (dashed line), is only a few fs. Therefore both maxima in the figure are nearly indistinguishable. The accuracy of the time correction can also be estimated from Eq. (25). An error to time zero is negligible near the pump wavelength, and it increases with detuning from the central frequency of the supercontinuum. The maximal error is of the order of $\max(|\omega_2-\Omega_2|/4\beta\xi^2)$, which is ≈ 8 fs for the parameters used.

The specific shape of the electronic spike, with a positive maximum and negative wings before and after time zero, is caused by the sine dependence in Eqs. (25) and (26). The amplitude of the wings is determined from the condition that the time-integrated signal at any probe wavelength must be zero. This is because the electronic response $R_e(\Omega)$ is a real function; i.e., there is no net absorption in the nonresonant case. Using Eq. (13), one obtains

$$\int dt_d \Delta D_e(\omega_2,t_d) \sim -\operatorname{Im} R_e(\Omega=0)=0. \tag{28}$$

Finally, there is a special symmetry of the electronic contribution relative to Ω_2, which is connected with the linear chirp. When substituting $(\Omega_2-\omega_2)\rightarrow(\omega_2-\Omega_2)$ and $t_d\rightarrow -t_d$, the signal remains the same, as is seen from Eq. (23) and from Fig. 1.

In practice, the electronic signal can be well fitted by the cross-correlation function and its time derivatives as [50]

$$\Delta D(\omega_2,t_d)=c_1F_{\rm cc}(\omega_2,t_d(\omega_2))+c_2F'_{\rm cc}(\omega_2,t_d(\omega_2)) + c_3F''_{\rm cc}(\omega_2,t_d(\omega_2)), \tag{29}$$

where $t_d(\omega_2)$ is given by Eq. (11). This can be obtained directly by expanding Eq. (25).

For *NC probe pulses*, $\beta=0$, and Eq. (23a) becomes

$$\Delta D_e(\omega_2,t_d)=-K\exp\left[-\frac{t_d^2}{\tau_1^2(1+2\xi^2)}\right] \times\sin\left[\frac{2\xi^2}{1+2\xi^2}t_d(\omega_2-\Omega_2)\right], \tag{30}$$

where $K=D_e^0\exp[\xi^4\tau_1^2(\omega_2-\Omega_2)/(1+2\xi^2)]$. If $\xi=\tau_2/\tau_1\ll 1$, which is of particular interest for a hole-burning experiment [1,2,5], Eq. (30) simplifies to

$$\Delta D_e(\omega_2,t_d)\approx -D_e^0\exp(-t_d^2/\tau_1^2)\sin[2\xi^2t_d(\omega_2-\Omega_2)]. \tag{31}$$

Simulations are shown in Fig. 3 for parameters $\xi=0.1$, $\tau_1=50$ fs, and $\tau_2=5$ fs, which are close to the experimental conditions in Refs. [1,2,5]. The simulated transient signal differs from that shown in Fig. 2. First, the calculated signal at true time zero is *zero* for any probe wavelength. Second, the coherent spike is always antisymmetric in time. Third, the amplitude of the signal is *zero* at central probe frequency $\omega_2=\Omega_2$ and increases with spectral detuning. Again, as for linearly chirped probing, the spike is antisymmetric relative to Ω_2. Note that apparent oscillations of the electronic signal in Fig. 3 should not be confused [51] with nuclear oscillations excited by the impulse-stimulated Raman-scattering (ISRS) process discussed below.

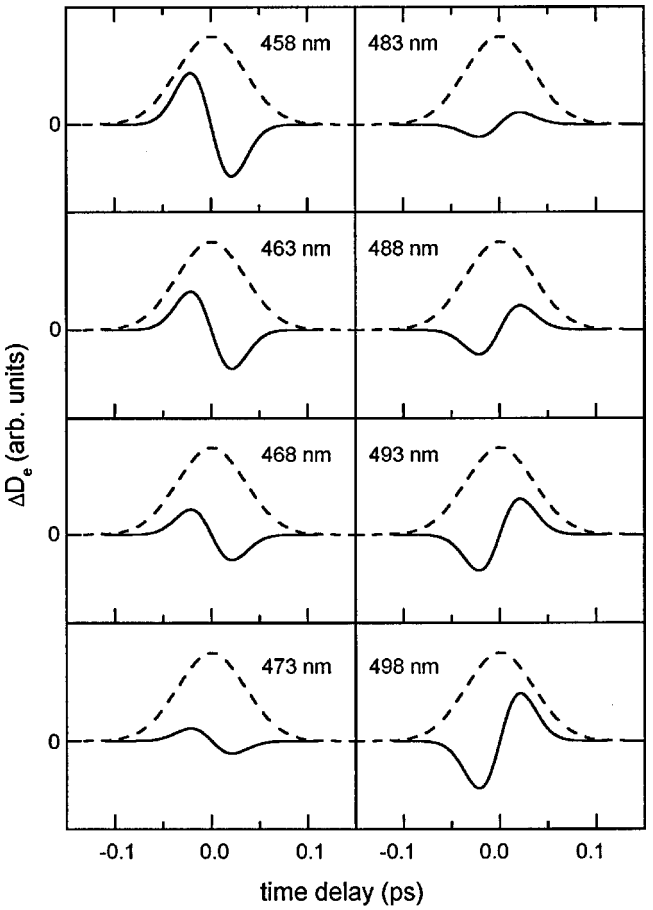

FIG. 3. Same as in Fig. 2, but the electronic signal $\Delta D_e(\omega_2,t_d)$ is simulated for NC probing with Eq. (30) for $\tau_2=5$ fs.

2. Impulsive-stimulated Raman-scattering contribution

This contribution to the nonresonant signal arises from low-frequency vibrations excited by an ultrashort pump pulse [52,53] and enters through the first term in Eq. (12a). We begin with the underdamped case $\gamma_n<\omega_n$. The corresponding response function has the form [47]

$$R_n(t)=\sigma_n\exp(-\gamma_nt)\sin\omega_nt, \tag{32a}$$

$$R_n(\Omega)=\mathcal{T}(R_n(t))=\frac{\sigma_n}{2}\left(\frac{1}{i\gamma_n+\omega_n-\Omega}-\frac{1}{i\gamma_n-\omega_n-\Omega}\right). \tag{32b}$$

Using Eqs. (13a) and (32b), the ISRS signal can be written as

$$\Delta D_{\rm ISRS}(\omega_2,t_d)=(D_n^0/2) \times\operatorname{Re}\{[W(z_1)-W(z_2)]\exp(B^2/4A)\}. \tag{33}$$

Here $D_n^0=2\omega_2\tau_1\sqrt{\pi}|a_1|^2\sigma_n$, $z_{1,2}=i\gamma_n\sqrt{A}-B/2\sqrt{A}\pm\omega_n\sqrt{A}$, and parameters A and B are defined by relations (13c) and (13d). We discuss now several limiting cases when Eq. (33) can be simplified.

Overlapped pump and probe pulses $[t_d+t_0(\omega_2)\to 0]$. In this case, $|z|\ll 1$, $W(z)\approx 1+i2z/\sqrt{\pi}$, giving

$$\Delta D_{\mathrm{ISRS}}(t_d\to 0)\approx -(2D_n^0/\sqrt{\pi})\mathrm{Im}[\omega_n\sqrt{A}\exp(B^2/4A)]. \tag{34}$$

By comparing with Eq. (23a) for the electronic contribution, we see that in this region of time delays the ISRS signal reproduces the shape of the electronic response. Therefore a time correction can be performed with the ISRS contribution if the electronic signal is smaller in magnitude.

Well-separated pulses. For $t_d+t_0(\omega_2)\gg\tau_1$, $|z|\gg 1$, and $W(z)\approx 2\exp(-z^2)$, the ISRS signal becomes

$$\Delta D_{\mathrm{ISRS}}\approx D_n^0\,\mathrm{Re}\{\exp(\Phi)[\exp(-i\omega_n\Psi)-\exp(i\omega_n\Psi)]\}. \tag{35}$$

Here $\Phi\equiv\Phi_1+i\Phi_2=-A(\omega_n^2-\gamma_n^2)+i\gamma_nB$ and $\Psi\equiv\Psi_1+i\Psi_2=2\gamma_nA+iB$. The final expression for the signal is

$$\begin{aligned}\Delta D_{\mathrm{ISRS}}\approx{}& 2D_n^0\exp(\Phi_1)\sqrt{\sin^2\Phi_2+\sinh^2\omega_n\Psi_2}\\ &\times\mathrm{sgn}(\cos\Phi_2\sinh\omega_n\Psi_2)\\ &\times\sin\{\varphi-(\mathrm{sgn}[\tan\Phi_2\coth\omega_n\Psi_2])\\ &\times\omega_n[t_d+t_0(\omega_2)]\},\end{aligned} \tag{36a}$$

$$\begin{aligned}\varphi={}&[\mathrm{sgn}(\tan\Phi_2\coth\omega_n\Psi_2)](\omega_n\gamma_n\tau_1^2/2)(1+2\xi^2/|\alpha|^2)\\ &+\arcsin(|\cos\Phi_2\sinh\omega_n\Psi_2|/\sqrt{\sin^2\Phi_2+\sinh^2\omega_n\Psi_2}).\end{aligned} \tag{36b}$$

In the case of *NC probe pulses*, $\beta=0$, $\alpha=1$, $\Psi_2=\tau_2^2(\omega_2-\Omega_2)$, and $\Phi_2=\gamma_n\Psi_2$. If in addition $\omega_n\gamma_n\tau_1^2\ll 1$, $\xi\ll 1$, the phase φ becomes $\varphi\approx\pi/2$ and the signal simplifies to

$$\Delta D_{\mathrm{ISRS}}\approx C_1(\omega_2-\Omega_2)\exp(-\gamma_nt_d)\cos(\omega_nt_d). \tag{37}$$

Here the coefficient $C_1=2D_n^0\tau_2^2\omega_n\exp[-\tau_1^2(\omega_n^2-\gamma_n^2)/4]$ reflects the amplitude dependence on the pump pulse duration. Note that the amplitude of oscillations changes linearly with detuning from the central frequency Ω_2; it is positive when $\omega_2>\Omega_2$ and negative for $\omega_2<\Omega_2$. This may be treated as inversion of the phase of oscillations at zero detuning [52].

Next, we consider *SC probing* assuming linear chirp. For $\gamma_n\ll\omega_n<1/\tau_1$, i.e., for an underdamped mode which is impulsively excited, one obtains, from Eq. (36a),

$$\Delta D_{\mathrm{ISRS}}(\omega_2,t_d)\approx C_1\exp\{-\gamma_n[t_d+t_0(\omega_2)]\}\mathrm{sgn}(\omega_2-\Omega_2)\sqrt{(\beta\tau_2^4\omega_n^2/|\alpha|^2)^2+[\omega_n\tau_2^2(\omega_2-\Omega_2)/|\alpha|^2]^2}\,\sin\{\omega_n[t_d+t_0(\omega_2)]\}. \tag{38}$$

The amplitude factor has a square-root dependence on detuning from Ω_2. This dependence is weak since the second term under the square root is smaller than the first term for detuning up to 4000 cm^{-1}. Note that the phase of oscillation is shifted by $\pi/2$ compared to the case of NC probe pulses [52].

3. Raman contribution

The Raman contribution $\Delta D_R(\omega_2,t_d)$ is given by the second term in Eq. (12a) together with the nuclear part of the response in Eq. (22). It can be also obtained from Eq. (16b) as

$$\begin{aligned}\Delta D_R(\omega_2,t_d)={}&D_R^0\,\mathrm{Re}\{(1/\sqrt{2\delta})\\ &\times[W(z_1)-W(z_2)]\exp(B^2/4A)\},\end{aligned} \tag{39}$$

where, as before, $z_{1,2}=i\gamma_R\sqrt{A_1}-(B_1/2\sqrt{A_1})\pm\omega_R\sqrt{A_1}$, $A_1=2A/\delta$, $B_1=[4A(\omega_2-\Omega_1)-B]/\delta$, $\delta=1+\xi^2/\alpha$, and $D_R^0=2\omega_2\tau_1\sqrt{\pi}|a_1|^2\sigma_R$. When deriving Eq. (39), $\omega_R\gg 1/\tau_1$ was assumed. Close to the resonances $\omega_2=\Omega_1\pm\omega_R$, Eq. (39) reads

$$\begin{aligned}\Delta D_R(\omega_2,t_d)\propto{}&\exp\{-[t_d+t_0(\omega_2)]^2/\tau_1^2\}\mathrm{Im}(1/z_1-1/z_2)\\ ={}&\exp\{-[t_d+t_0(\omega_2)]^2/\tau_1^2\}\\ &\times\left[\frac{\gamma_R}{\gamma_R^2+(\omega_2-\Omega_1-\omega_R)^2}\right.\\ &\left.-\frac{\gamma_R}{\gamma_R^2+(\omega_2-\Omega_1+\omega_R)^2}\right].\end{aligned} \tag{40}$$

This expression is valid both for chirped and NC probing [in

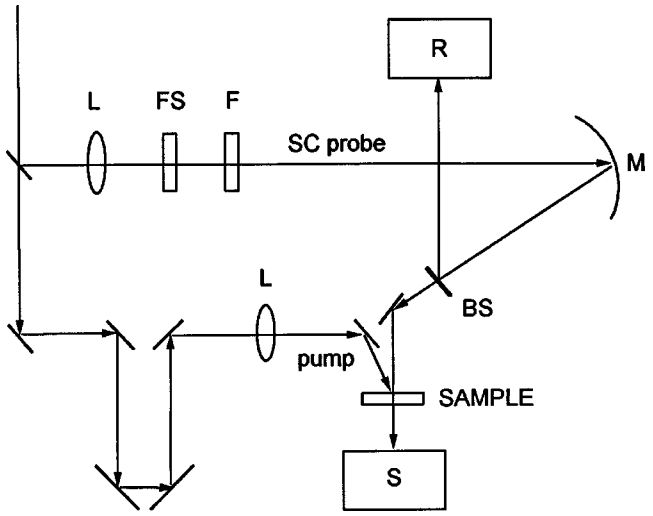

FIG. 4. Scheme of the experimental setup. For details, see Sec. III A.

the last case $t_0(\omega_2)\equiv 0$]. As is readily seen, there is an emission (negative signal) at the Stokes frequency $\omega_2=\Omega_1-\omega_R$ and an absorption (positive signal) at the anti-Stokes side $\omega_2=\Omega_1+\omega_R$. The evolution of the transient signal reproduces the cross correlation between the pump and SC probe, with a width of τ_1, for $2\beta\tau_1^2>1$. Since for a strong Raman mode this signal is usually much higher than the electronic contribution, it allows direct measurement of the cross correlation at some fixed frequencies.

Note that Eq. (40) is also relevant for two-photon absorption $\omega_{2\mathrm{ph}}=\Omega_1+\omega_2$, when formally substituting $\omega_2\rightarrow -\omega_2$, $\omega_R\rightarrow -\omega_{2\mathrm{ph}}$, and keeping only the first term in square brackets.

In the following experimental section, we compare the above theoretical estimates with experimental results on fused silica and several pure solvents. We also illustrate the PSCP technique by resonant transient spectroscopy of the dye DCM in acetonitrile.

III. EXPERIMENTAL RESULTS AND DISCUSSION

A. Experiment

A scheme of the experimental setup is shown in Fig. 4. The laser system is based on a distributed feedback dye laser [18,54] which operates at a 2-Hz repetition rate. It produces basic pulses with a duration of 50 fs and energy of 50 μJ, centered at 450, 480, or 530 nm. The fundamental beam is split into two parts. The first, after passing a variable delay stage, is used for optical pumping. The diffraction-limited beam has a diameter of 100–120 μm on the sample with a pulse energy of 0.5–2.0 μJ. The second part, with an energy of 10–20 μJ, is focused with a 200-mm lens (L) into a fused silica plate (FS), of 2 mm thickness, to generate supercontinuum probe pulses. The supercontinuum is flattened spectrally by a homemade filter (F). This is a fused silica cuvette with 0.16-mm-thick windows, filled by a mixture of dyes dissolved in methanol. The full thickness of the filter is 0.6 mm. The quality of the supercontinuum, its stability and spectral smoothness, depends critically on the pump pulse energy, pump beam diameter, and focusing parameter. The best supercontinuum, spectrally broad and smooth, is produced when working at distances slightly larger than the focal length and with higher pump energy. However, this leads to an undesirable increase of the spot size on the sample.

The supercontinuum pulses, with an energy <0.1 μJ, are imaged onto the sample by dispersion-free anastigmatic optics (M). The pump and probe beams intersect at the sample with an angle of 5°, the probe diameter being 80–100 μm. The sample net thickness is 0.3 mm, and the fused silica windows (Suprasil I) are 0.16 mm thick. The solution is flown out of the interaction region after each laser shot. All measurements are performed with parallel pump-probe polarization (except for chloroform). After interaction with the sample, the supercontinuum is dispersed by a polychromator (S) to obtain the signal spectrum $I_s(E_1)$ which is registered on a photodiode array with 512 pixels (Hamamatsu). A part is split off before interaction and is dispersed and registered separately (R) for reference I_r. The differential optical signal $\Delta D_{\mathrm{expt}}(\omega_2,t_d)$ is obtained as

$$\Delta D_{\mathrm{expt}}(\omega_2,t_d)=-\log_{10}[I_s(E_1)/I_s(0)], \qquad (41)$$

where $I_s(0)=I_r(I_s^B/I_r^B)$, and I_s^B and I_r^B are obtained from a special base-line measurement for which the pump is switched off. During the experiment, the base line is corrected every ten time steps. ΔD_{expt} is given by Eq. (2) multiplied by $\ln 10\approx 2.3$, under the condition $\Delta D_{\mathrm{expt}}<0.1$. Typically, 10–20 measurements are averaged to give a wavelength-dependent signal at every time step of 6.67 fs. The transient spectra are recorded in the range of 350–800 nm with a resolution of 1.5 nm. We estimate the absolute error for ΔD_{expt} as 0.003.

The intensity autocorrelation of the pump was measured in the same geometry when replacing the sample by a 0.1-mm-thick BBO crystal. Its full width at half maximum (FWHM) of 65–75 fs (depending on the wavelength of the pump pulse and other experimental conditions) corresponds to 45–54-fs pulses; the noncollinear geometry contributes an estimated 15 fs to the measured correlation width. The spectral width of the pump pulses of 11–12 nm (400 cm^{-1}) gives a lower limit to the pulse duration of 35 fs.

Solvents (Merk) and the dye DCM (4-dicyanomethylene-2-methyl-6-*p*-dimethylaminostyryl-4H-pyran, Lambda Physik) were used as received. All measurements were performed at ambient temperature.

B. Results and discussion

1. Nonresonant PSCP spectroscopy

We start with the results obtained from two 0.16-mm-thick fused silica windows (empty probe cell). Figure 5 shows the experimental signal $\Delta D_{\mathrm{expt}}(\omega_2,t_d)$ (circles) measured at different probe wavelengths. The behavior of the signal is in good agreement with simulations of pure electronic response shown in Fig. 2 for a linearly chirped SC. The positive maximum of the signal shifts in time with probe wavelength, which reflects the chirp of the experimental supercontinuum. A characteristic shape of the signal, including details like a specific asymmetry of the spike on the blue and red edge of the spectrum, is consistent with Fig. 2.

A more quantitative treatment can be further obtained by measuring $t_0(\omega_2)$ and then by fitting the experimental data with Eq. (26) or (29). The best fit is shown in Fig. 5 by solid lines through the experimental points; fitting parameters are the time-zero function $t_0(\omega_2)$, the cross-correlation width τ_{cc}, and the amplitude of the signal. The spectral dependence of these parameters is displayed in Figs. 6(b)–6(d). Figure 6(a) shows the experimental supercontinuum [which is used for approximating the signal by Eq. (12)] and the location of the pump pulse. As is seen from Fig. 6(b), the chirp of the supercontinuum is nearly linear, with a weak overshoot at the pump wavelength. The cross-correlation width τ_{cc} is between 60 and 70 fs over the whole spectral range. Equation (27) predicts the smaller width of 50 fs. This deviation may be due to propagation effects in the sample, which were neglected in theoretical section.

A first estimate for $t_0(\omega_2)$ can be obtained directly from the kinetic traces, by locating the positive maximum of the signal by inspections and then smoothing the obtained spectral dependence. This procedure gives a good approximation to $t_0(\omega_2)$ with an accuracy better than ± 15 fs. In the fit, this parameter and the cross-correlation width τ_{cc} are allowed to vary within this uncertainty. As a result, the excellent fit of

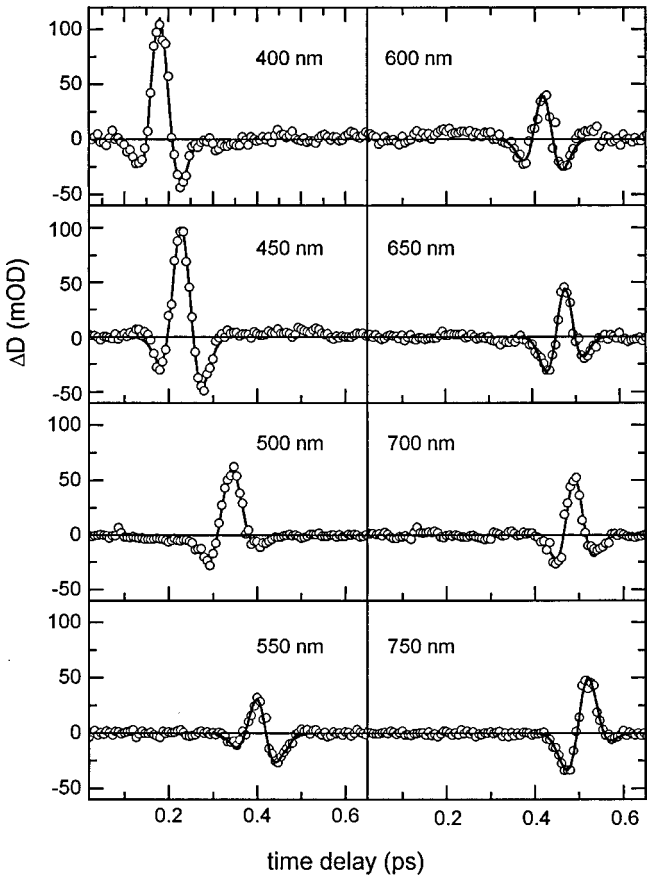

FIG. 5. Circles: experimental PSCP signal $\Delta D_{\mathrm{expt}}(\omega_2,t_d)$ obtained from two fused silica windows 0.16 mm thick, with pump energy of 1.6 μJ centered at 476 nm. Solid lines: the best fit of the signal with Eq. (26). The spectrum of the experimental supercontinuum and the fitting parameters $t_0(\omega_2)$ together with the cross-correlation width $\tau_{\mathrm{cc}}(\omega_2)$ are shown in Fig. 6. (OD denotes optical density.)

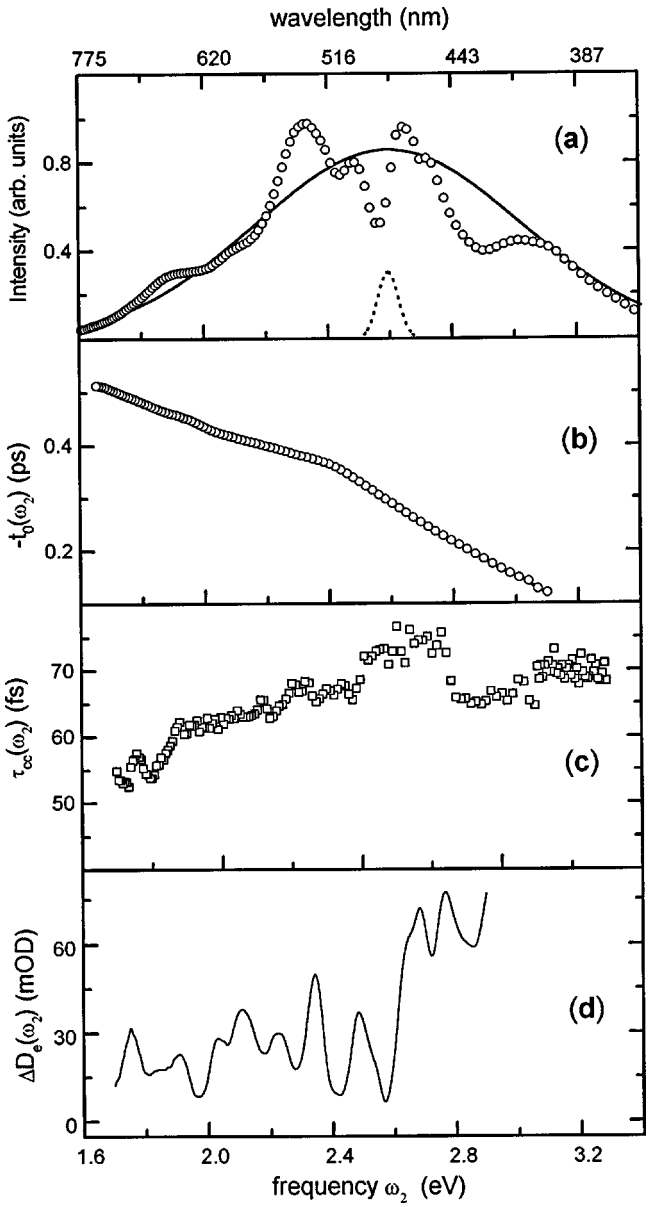

FIG. 6. (a) Power spectrum of the experimental supercontinuum (circles) and its approximation by a linearly chirped pulse (solid line). The spectrum of the excitation pulse is drawn by a dashed line. (b) Time-zero function $t_0(\omega_2)$ (with an experimental offset). (c) Cross-correlation width $\tau_{\mathrm{cc}}(\omega_2)$. (d) Amplitude of the electronic signal as derived from the experimental data of Fig. 5.

the experimental signal is obtained. A main conclusion which can be drawn from Figs. 5, 6(b), and 6(c) is that the experimental SC can be well described as a *single* nonlinearly chirped pulse, its phase being determined from the $t_0(\omega_2)$ dependence by Eqs. (9) and (10). The spectral dependence of the amplitude of the signal is shown in Fig. 6(d). On average, the amplitude increases with decreasing probe wavelength. This agrees with the dispersive spectral behavior of the hyperpolarizability $\sigma_e(\omega_2)$ [49] for nonresonant excitation. In addition, it shows spectral gaps and peaks which may be attributed to Raman active modes of fused silica [55]. We shall come back to these features when we discuss the transient signal from pure acetonitrile.

The next set of experiments was performed with pure chloroform. Figure 7 shows time-corrected kinetic traces for different wavelengths with perpendicular (a) and parallel (b) pump-probe polarization. Underdamped oscillations, excited by impulsive stimulated Raman scattering of the pump pulse (at 478 nm), are seen over the whole spectral range of probing. Fourier spectra of the signal, averaged over the spectral range from 420 to 700 nm, are shown in Fig. 8. They result in two prominent modes [56] at 367 and 667 cm^{-1}. A mode at 260 cm^{-1}, which is pronounced in Kerr-effect studies [57], is also visible but its intensity is much lower compared to the fully symmetric 367-cm^{-1} mode. A small peak at 415 cm^{-1} is probably due to a Raman-active mode of fused silica [55].

The spike around time zero in Fig. 7 corresponds to the electronic response, as in the case of fused silica. The amplitude of the spike for perpendicular polarization is decreased approximately by a factor of 3 compared to the case of parallel polarization. This is consistent with the symmetry properties of the hyperpolarizability tensor [46]. The relative intensities of the electronic spike and of the amplitude of oscillations are directly seen from Fig. 7. It confirms earlier findings [48,49] that the electronic response is considerably higher than the ISRS contribution, even for most prominent low-frequency modes. Solid lines through the experimental points show a fit of the total signal with Eq. (38). The phase

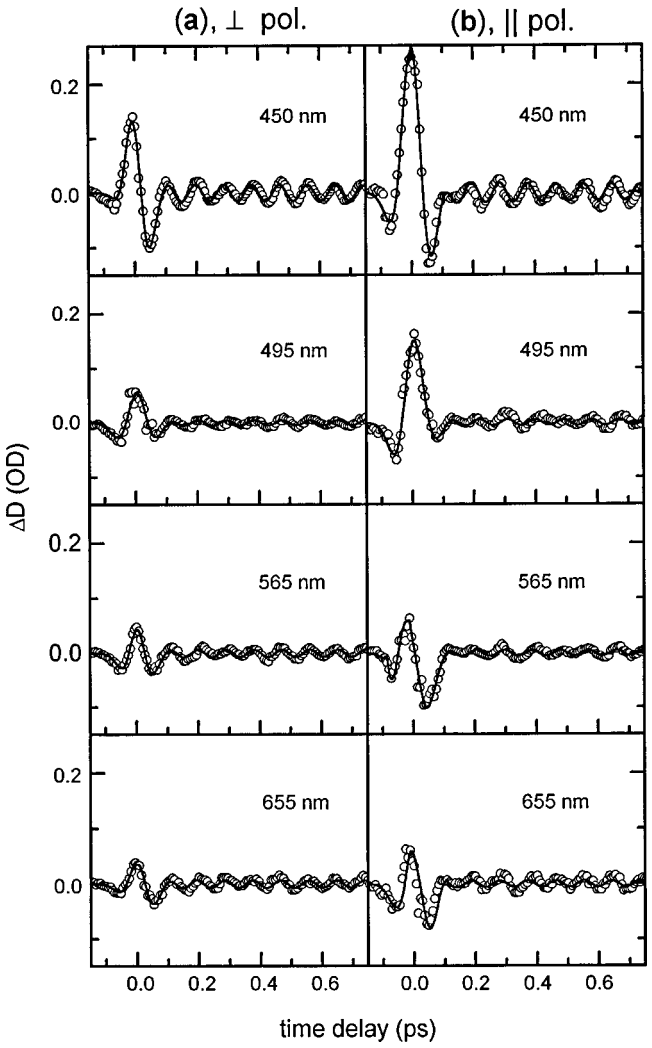

FIG. 7. Time-corrected PSCP signal (circles) from pure chloroform for perpendicular (a) and parallel (b) polarization between the pump and SC probe. Solid lines show the best fit with both the electronic [Eq. (29)] and ISRS [Eq. (38)] contributions. Only the dominant 367-cm^{-1} mode is included in the fit. Probe wavelengths are given as insets.

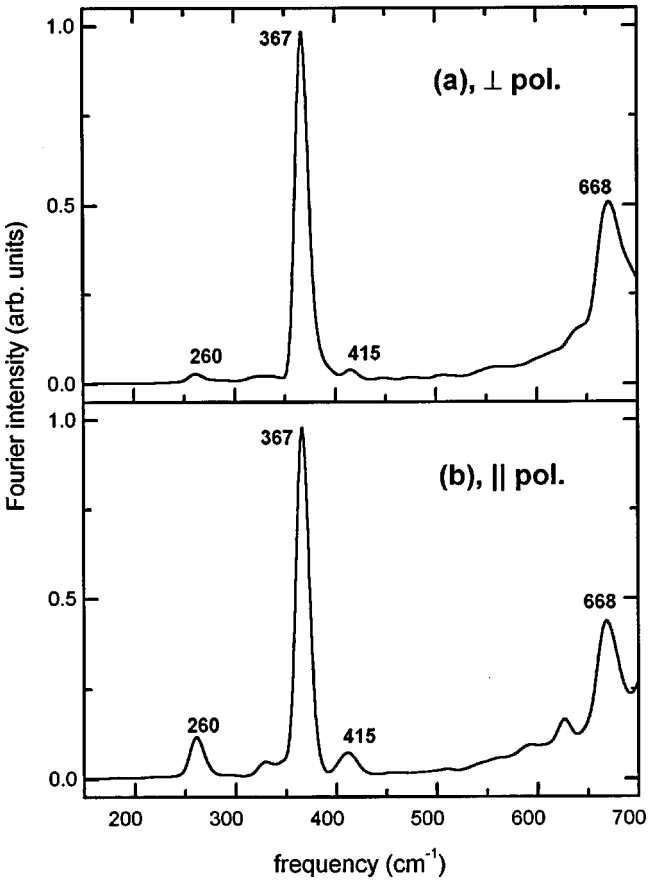

FIG. 8. Power spectral density of the ISRS oscillations (the electronic contribution is excluded) shown in Fig. 7, averaged over the probe spectral range 450–700 nm.

of the oscillations and their decay rate obtained from this fit are plotted in Fig. 9 in the spectral range 450–750 nm. The averaged decay time of the oscillations is $\approx$3 ps. The phase is close to zero as predicted by Eq. (38); the deviation of $(2\pi/8)$ reflects our accuracy of 10 fs in determining $t_0(\omega_2)$. In principle, the obtained spectral dependence can be used to improve the time-zero correction.

We conclude this subsection with experimental results on pure acetonitrile. Figure 10 shows time-corrected kinetic traces at fixed probe wavelengths which were measured with the pump pulse centered at 450 nm. New features here are strong Raman contributions from CH (2950 cm^{-1}) and CN (2250 cm^{-1}) stretching modes [56] of pure acetonitrile. The CH mode is seen as anti-Stokes absorption at 396 nm and as Stokes emission at 518 nm in accordance with Eq. (40). Similarly, the CN mode gives the signal at 408 and 498 nm. At these wavelengths the Raman contribution is comparable in magnitude to the electronic response. This results in a complicated shape of the signal at 498 mn where the two contributions have opposite sign. The strong CH mode gives a signal which is much higher than the electronic response. Therefore the pump-probe cross-correlation width τ_{cc} can be measured directly at the corresponding wavelengths of 396 and 518 nm. This gives 60 and 50 fs, respectively.

The Raman part of the transient signal is best seen in the frequency domain. The dotted line in Fig. 11 represents the time-corrected spectrum of pure acetonitrile at zero delay. Here the electronic response is recognized as a positive background, while the Raman contributions are seen as peaks and gaps for positive and negative detunings from the pump frequency. Generally, the behavior of the signal is similar to that shown in Fig. 6(d) for fused silica. However, for fused silica, the electronic response is dominant (the total signal is positive for all probe frequencies), while for acetonitrile the Raman part is much more pronounced, so that a negative signal is observed at negative detuning.

A further step in the analysis of the Raman contributions can be taken by integrating the experimental transient spectra over time around zero delay. As predicted by Eq. (28), the electronic contribution vanishes in this case and the integrated signal is exclusively due to Raman modes. In Fig. 11, the time-integrated (from -150 to 250 fs) spectrum is shown as a solid line. Indeed, the signal is now antisymmetric relative to zero detuning, as is expected for a pure Raman spectrum, the modes [56] at 900 and 1400 cm^{-1} being much better visible. It is interesting that the 380-cm^{-1} mode, seen as oscillations in the time domain [57] (and also in our pump-probe measurements which are not shown here), ap-

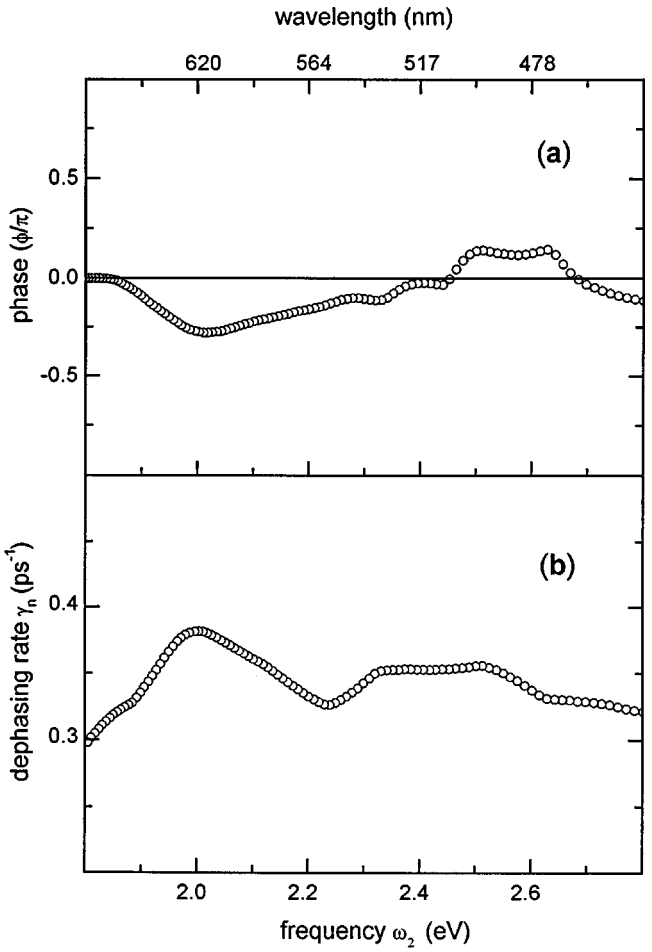

FIG. 9. (a) Spectral dependence of the phase φ and (b) decay rate γ_n of the 367-cm^{-1} mode seen as oscillations in Fig. 7. The fit is obtained with Eq. (36).

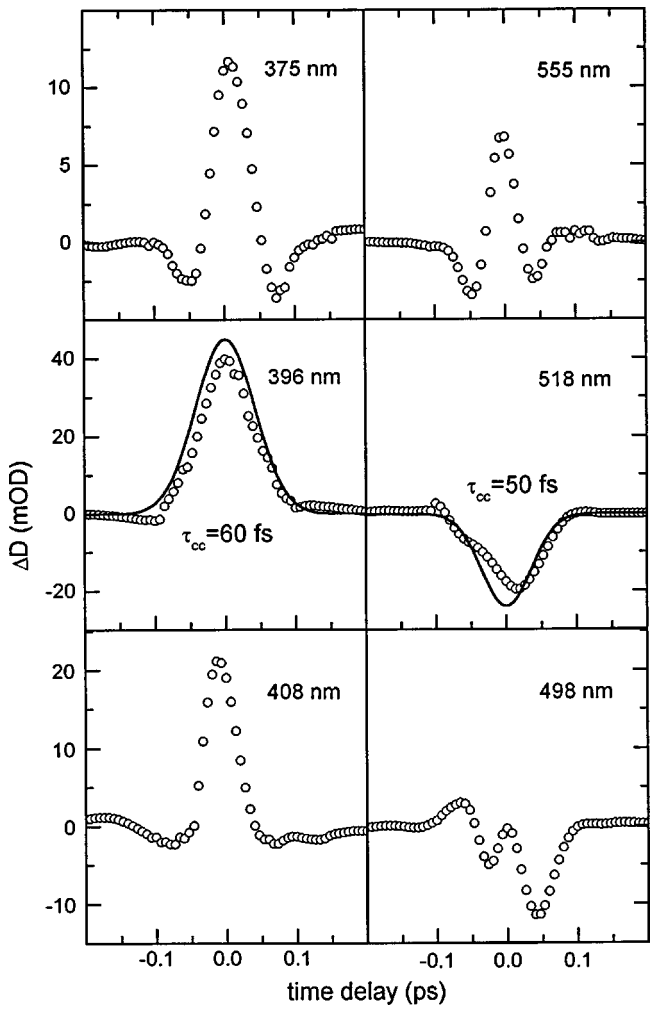

FIG. 10. Time-corrected PSCP signal $\Delta D_{\mathrm{expt}}(\omega_2,t_d)$ from pure acetonitrile. The pump is centered at 450 nm. Probe wavelengths are shown as insets. The Raman contribution due to the CH-stretching mode at 2950 cm^{-1} is seen at 396 nm (anti-Stokes absorption) and at 518 nm [Stokes emission; cf. Eq. (40)].

pears in the frequency domain similar to higher frequency modes, with its amplitude negative (positive) for negative (positive) detuning. Thus an apparent π jump of the phase of oscillations, when crossing zero detuning [52], can be explained as a change from emission to absorption.

Now we turn to the resonant PSCP spectroscopy of the dye DCM in solution [21].

2. Resonant PSCP spectroscopy of the dye DCM in acetonitrile

Figure 12(a) shows the stationary absorption and emission spectra of DCM in acetonitrile. The Stokes shift between the absorption and emission band is $\approx$6000 cm^{-1}. The pump pulse at 531 nm is adjusted to a far red edge of the absorption band to excite only the $0''\rightarrow 0'$ vibronic transition and, hence, to avoid vibrational relaxation in the excited state just after pumping. Time-corrected transient absorption spectra are shown in Fig. 12(b) from 0 to 60 fs in 20-fs steps and from 80 to 400 fs in 40-fs steps (c). Before 60 fs, when pump and probe pulses overlap, prominent spectral structure is observed, which can be explained as follows. The spectral gaps at 629 and 603 nm (and the peaks at 460 and 473 nm) are due to nonresonant Raman scattering from pure acetonitrile, as is evident by comparison with Fig. 11. At these wavelengths, the solvent contribution is comparable to the resonant part of the signal. For other spectral regions, the solvent signal is relatively small even at early time; hence, the rest of the structure can be assigned to the solute. This spectral structure can be well described by a single vibrational mode with frequency of 1550 cm^{-1}, which is active both in the ground and excited states. In this picture, the gap at the pump wavelength corresponds to a $0'\rightarrow 0''$ transition and contains three contributions [6–8,15,21]: (i) from the population ''hole'' created by pumping in the ground electronic state, (ii) from the population ''particle'' in the excited state, and (iii) due to coherent (Raman) processes. The redshifted gap at 580 nm corresponds to the $0''\rightarrow 1'$ transition from the particle and contains contributions (ii) and (iii). Similarly, the blue shifted gap corresponds to the $0'\rightarrow 1''$ transition from the hole and contains contributions (i) and (iii). The dominant vibrational mode is seen as a Franck-Condon progression in the far-red part of the spectrum, at 687 nm, where it contributes through the $0''\rightarrow 3'$ transition. Although the signal is small there, it is well reproducible for different experimental conditions. There must also be a contribution from the same mode around 630 nm ($0''\rightarrow 2'$ transition), but here it is masked by the solvent signal.

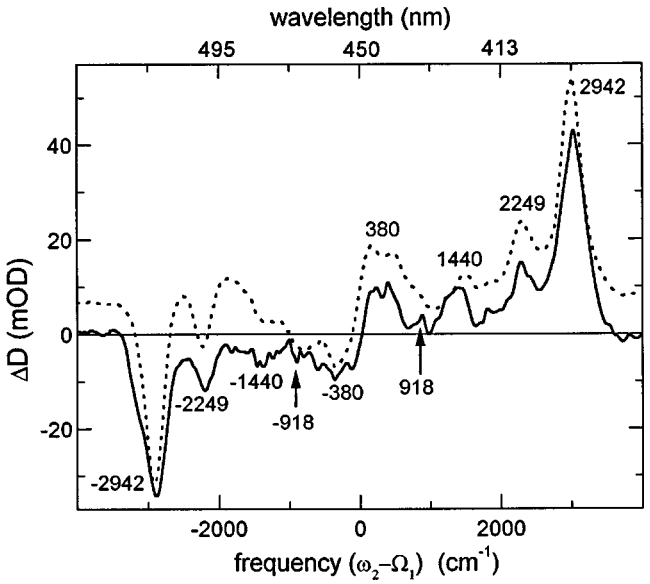

FIG. 11. Time-corrected transient spectrum of pure acetonitrile at zero delay (dotted line) and the time-integrated spectrum from −150 to 250 fs (solid line). This integration removes the electronic contribution [cf. Eq. (28)].

It is interesting to compare the transient spectra of Fig. 12(b) with those measured by Brito Cruz *et al.* [1] for another dye, cresyl violet in ethylene glycol. These workers applied 10-fs NC probe pulses to observe a spectral structure in their transient spectra, which was due to a 600-cm^{-1} intramolecular vibrational mode of cresyl violet. In our experiment, we are capable of obtaining similar results with SC probing for which the total pulse duration is a few hundred fs.

The spectral evolution of the transient signal at later time, from 80 to 400 fs, is displayed in Fig. 12(c). The signal decreases in the range $500<\lambda<590$ nm and increases in the red part of the spectrum, showing an isosbestic point at 590 nm. This indicates [21] a state-to-state intrachromophore relaxation process with a time constant of 140 fs. It is interesting that in the blue part of the spectrum ($\lambda<490$ nm), where the excited state absorption is dominant, the signal stays constant in time. This suggests that whichever relaxation processes take place in the excited electronic state, the spectral evolution of the signal in the red part ($\lambda>490$ nm) is not influenced by the excited-state absorption.

Relevant information concerning intramolecular relaxation processes can be also obtained from the time domain. Figure 13 shows kinetic traces from 520 to 630 nm with 10-nm steps. Here the pump pulse is tuned to 470 nm, close to the absorption maximum. Underdamped oscillations of the transient signal are clearly visible up to 1 ps. By chance, their frequency of 392 cm^{-1} is close to that in pure acetonitrile. Since these oscillations have been observed by us in methanol also, they are attributed to the excited chromophore. Figure 14 shows the spectral dependence of the amplitude of the oscillations. Note that the amplitude maximum is at 590 nm, which is also the location of the isosbestic point in Fig. 12. Although at present we have no explanation of this correlation, we show this result as an illustration of potential capabilities of the PSCP technique.

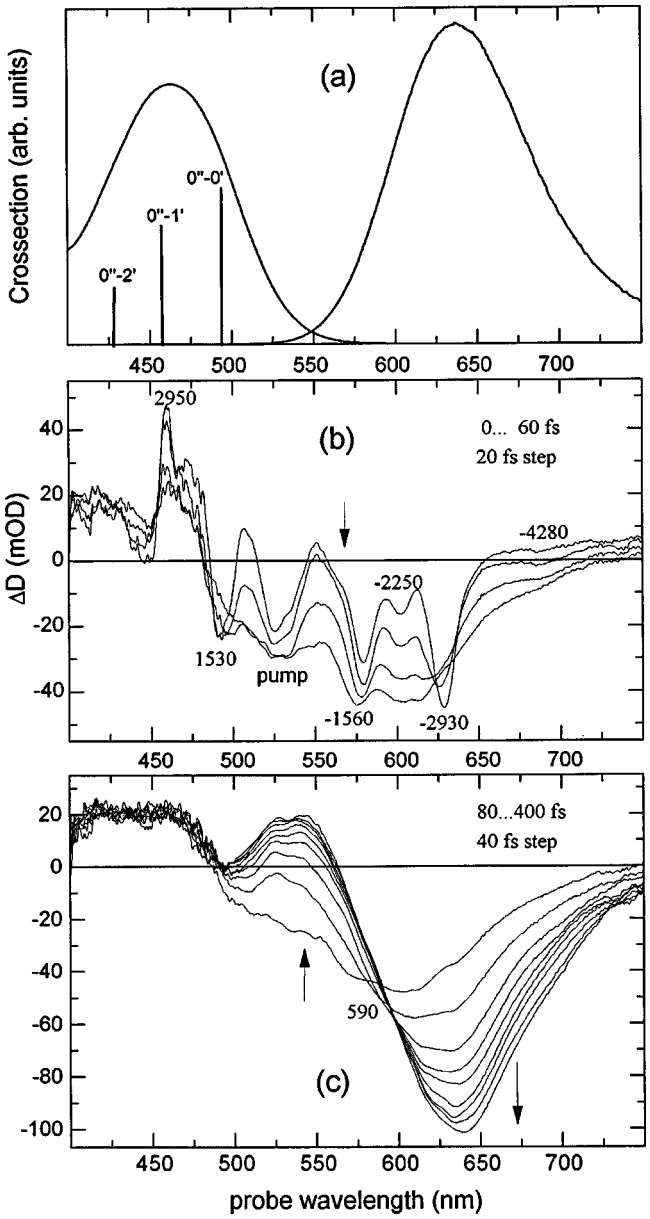

FIG. 12. (a) Absorption and stimulated emission spectra (for cross sections) of the dye DCM in acetonitrile. A stick spectrum of the dominant vibrational mode (1550 cm^{-1}) is also shown. (b) Transient spectra from 0 to 60 fs in 20-fs steps with SC probing after time correction. The pump pulse of 0.4 μJ is centered at 531 nm. The detuning of the spectral peaks and holes from the pump frequency is given in cm^{-1}. (c) Same as in (b), but from 80 to 400 fs in 40-fs steps. Arrows indicate the evolution of the signal.

IV. SUMMARY AND CONCLUSION

A. Characterization of the supercontinuum

One of the main results of this article deals with characterization of the supercontinuum. Starting with the representation of the SC probe as a single chirped pulse, we calculated the transient PSCP signal in the nonresonant case. Excellent agreement between the theoretical estimates and a whole body of experimental results on fused silica and pure solvents then proves the validity of our treatment. Furthermore, this provides criteria by which one can experimentally

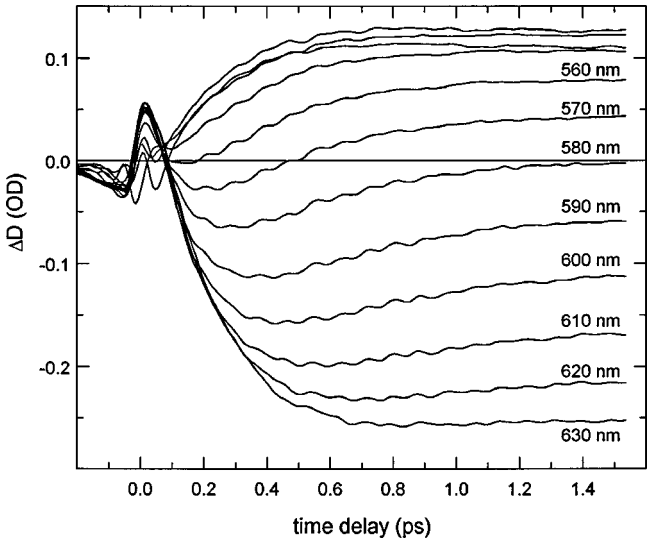

FIG. 13. Time-corrected kinetics for DCM in acetonitrile. Apparent oscillations, due to ISRS resonance excitation, are visible for probe wavelengths from 520 to 650 nm. The pump pulse of 1 μJ is tuned to 470 nm.

check the applicability of the supercontinuum for the PSCP spectroscopy. These criteria are the following: (1) the nonresonant transient signal must show a specific shape of the electronic response, and (2) high-frequency Raman modes must be seen on the Stokes and anti-Stokes sides from the pump wavelength. When these conditions are fulfilled, the supercontinuum is properly adjusted, and it can be fully characterized by its chirp through the $t_0(\omega_2)$ dependence and by its spectral shape, which is measured directly.

We stress the significance of the careful adjustment of the supercontinuum for obtaining high-quality transient spectra. Although practical recommendations for handling the supercontinuum were given in Sec. II B, the adjustment will be different for every individual experimental setup. In this respect, the above-mentioned criteria are of particular importance. Recently, Ranka *et al.* [58] observed splitting and spectral broadening of femtosecond pulses in transparent media. They assigned this phenomenon to an initial stage of supercontinuum generation when the energy of the input pulse is relatively low. This kind of supercontinuum can be recognized by its narrow spectral width and must be avoided in PSCP experiments.

As has been mentioned in Sec. I, the chirp of the supercontinuum and the cross-correlation width can be also measured by a nonlinear crystal, in accordance with Eq. (27). In this case, however, one must replace the sample by the crystal and then replace again the crystal by the sample. This operation disturbs the adjustment of the optical system and should be avoided. Also the phase-matching geometry for detecting the sum-frequency signal differs from that for the pump-probe experiment. Thus the registration channel must be readjusted completely or another registration system will be involved. It is also essential that the spectral intensity of the supercontinuum must be sufficiently low to exclude self-action of the probe field, which in turn prevents measuring the sum-frequency signal with a good signal-to-noise ratio. These and others technical complications lead to errors in determining $t_0(\omega_2)$ and $\tau_{cc}(\omega_2)$. Our method is free from

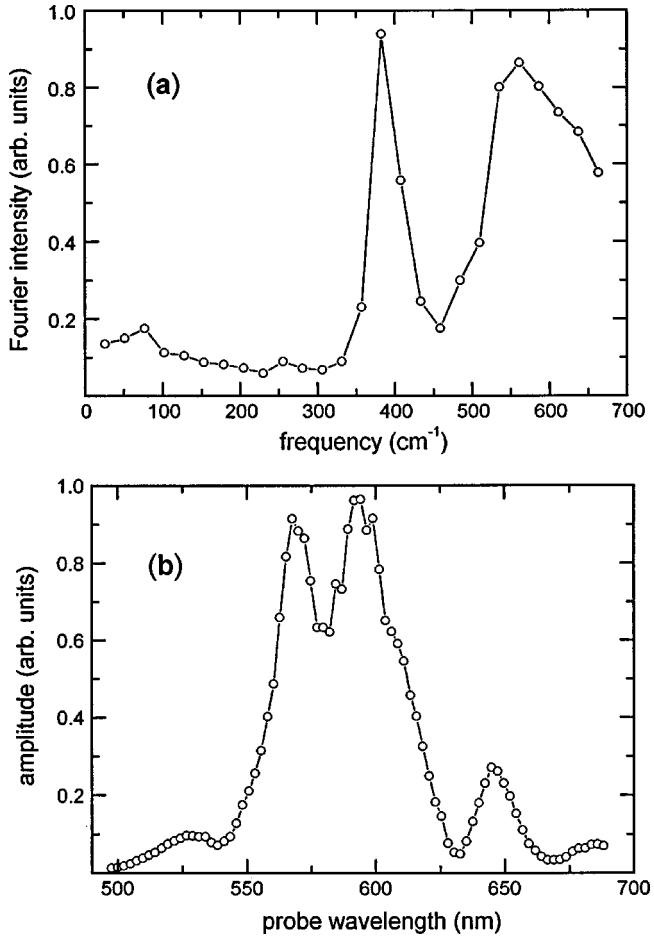

FIG. 14. (a) Averaged power spectrum of the oscillations seen in Fig. 13 and (b) amplitude of the dominant 392-cm^{-1} mode of the oscillations as a function of the probe wavelength.

these disadvantages, and it allows the characterization of the supercontinuum exactly at the same conditions as for pump-probe measurements. In addition, the measured pure solvent (substrate) signal can be subtracted from the total to obtain the transient absorption spectra exclusively from the sample.

B. Time-zero correction and early transient spectra

The next important point concerns the theoretical treatment of the PSCP experiment in the resonance case. We have shown in Sec. II B that for a relatively slow response function $R(t)$ [when $R'(t)/R(t) < 1/(20\,\text{fs})$], the time-corrected transient spectra reproduce those obtained with spectrally tunable nonchirped probe pulses. Thus theories [2,5–11] of pump-probe measurements, developed earlier for NC pulses, can be applied as they are. For a fast response function, the time-correction procedure also gives qualitative insight into the early time behavior, but the transient signal should be calculated with Eq. (12).

The accuracy of time correction of $\approx$10 fs, which was experimentally achieved for this study, allows the analysis of early transient spectra such as shown in Fig. 12(b). On this time scale one may neglect slower intramolecular processes and consider only solvent relaxation (broadening) to be relevant. Then the signal can be calculated for a model response function, taking into account both coherent and sequential

(population) terms. Recently, Cong *et al.* [34] performed such calculations, in the frame of the Brownian oscillator mode [6], to treat their degenerate pump-probe experiment on the dye HITCI in ethylene glycol. The same approach can be applied in our case, with the advantage that the transient signal can now be fitted over the whole spectral range of probing. Thus early transient spectra of chromophors in solution can be used as a test for theories of solvation.

Finally, the time-zero problem exists even for nonchirped probing, as it is obvious from Fig. 3. Monitoring the nonresonant electronic response should provide precise timing in this case also. For 10-fs pump and probe pulses, one may expect an accuracy of timing of 0.5 fs. This will allow precise measurements of the phase of oscillations, resonantly excited in the probe molecule. As has been shown [43,59], this phase is sensitive to electronic dephasing processes.

In conclusion, we presented the theoretical and experimental background of the PSCP technique for transient broadband absorption spectroscopy with supercontinuum probing. With 50-fs pump pulses, the technique allows for analysis of experimental data both in the time and frequency domain with time resolution of 10 fs. We believe that with the clarification of inherent problems of the technique, as made in this article, the method will be widely used for ultrafast spectroscopy in condensed phases.

ACKNOWLEDGMENTS

We thank Professor S. Mukamel for valuable comments. We thank the Deutsche Forschungsgemeinschaft for support through the Leibniz Program and the Fonds der Chemischen Industrie for financial assistance. A.L.D. thanks the Russian Foundation for Basic Research for partial financial support.

[1] C. H. Brito Cruz, R. L. Fork, W. H. Knox, and C. V. Shank, Chem. Phys. Lett. **132**, 341 (1986).
[2] W. T. Pollard, C. H. Brito Cruz, C. V. Shank, and R. A. Mathies, J. Chem. Phys. **90**, 199 (1989).
[3] A. Mokhtari, A. Chebira, and J. Chesnoy, J. Opt. Soc. Am. B **7**, 1551 (1990).
[4] M. L. Horng, J. A. Gardecki, A. Papazyan, and M. Maroncelli, J. Phys. Chem. **99**, 17 311 (1995).
[5] W. T. Pollard, S-Y. Lee, and R. A. Mathies, J. Chem. Phys. **92**, 4012 (1990).
[6] Y. J. Yan and S. Mukamel, Phys. Rev. A **41**, 6485 (1990); S. Mukamel, Annu. Rev. Phys. Chem. **41**, 647 (1990).
[7] S. Kinoshita, J. Chem. Phys. **91**, 5175 (1989).
[8] R. F. Loring, Y. J. Yan, and S. Mukamel, J. Chem. Phys. **87**, 5840 (1987).
[9] B. D. Fainberg, Chem. Phys. **148**, 33 (1990).
[10] S. Mukamel, J. Chem. Phys. **107**, 4165 (1997).
[11] Y. J. Yan, W. Zhang, and J. Che, J. Chem. Phys. **106**, 2212 (1997); **106**, 6947 (1997).
[12] C. V. Shank, R. Yen, R. L. Fork, J. Orenstein, and Baker, Phys. Rev. Lett. **49**, 1660 (1982).
[13] R. R. Alfano and S. L. Shapiro, Phys. Rev. Lett. **24**, 584 (1970).
[14] R. L. Fork, C. V. Shank, C. Hirlimann, R. Yen, and W. J. Tomlinson, Opt. Lett. **8**, 1 (1983).
[15] T. J. Kang, J. Yu, and M. Berg, J. Chem. Phys. **94**, 2413 (1991).
[16] H. Murakami, S. Kinoshita, Y. Hirata, T. Okada, and N. Mataga, J. Chem. Phys. **97**, 7881 (1992).
[17] E. Lenderink, K. Duppen, and D. Wiersma, Chem. Phys. Lett. **194**, 403 (1992); J. Phys. Chem. **99**, 8972 (1995).
[18] D. Bingemann and N. P. Ernsting, J. Chem. Phys. **102**, 2691 (1995).
[19] K. Nishiyama, Y. Asano, N. Nashimoto, and T. Okada, J. Mol. Liq. **65/66**, 41 (1995).
[20] N. Eilers-König, T. Kühne, D. Schwarzer, P. Vöringer, and J. Schroeder, Chem. Phys. Lett. **253**, 69 (1996).
[21] S. A. Kovalenko, N. P. Ernsting, and J. Ruthmann, Chem. Phys. Lett. **258**, 445 (1996).
[22] M. G. Muller, M. Hucke, M. Reus, and A. R. Holzwart, J. Phys. Chem. **100**, 9527 (1996).
[23] S. A. Kovalenko, N. P. Ernsting, and J. Ruthmann, J. Chem. Phys. **106**, 3504 (1997).
[24] S. A. Kovalenko, J. Ruthmann, and N. P. Ernsting, Chem. Phys. Lett. **271**, 40 (1997).
[25] S. A. Kovalenko, J. Ruthmann, and N. P. Ernsting, J. Chem. Phys. **109**, 1894 (1998).
[26] C. L. Thomsen, J. Thogersen, and S. R. Keiding, J. Phys. Chem. A **102**, 1062 (1998).
[27] S. Yamagichi and H. Hamaguchi, J. Chem. Phys. **109**, 1397 (1998).
[28] Yu. E. Lozovik, A. L. Dobryakov, N. P. Ernsting, and S. A. Kovalenko, Phys. Lett. A **223**, 303 (1996).
[29] V. M. Farztdinov, A. L. Dobryakov, V. S. Letokhov, Yu. E. Lozovik, Yu. A. Matveets, S. A. Kovalenko, and N. P. Ernsting, Phys. Rev. B **56**, 4176 (1997).
[30] Z. Vardeny and J. Tauc, Opt. Commun. **39**, 396 (1981).
[31] B. S. Wherrett, A. L. Smirl, and T. F. Boggess, IEEE J. Quantum Electron. **QE-19**, 680 (1983).
[32] S. L. Palfrey and T. F. Heinz, J. Opt. Soc. Am. B **2**, 674 (1985).
[33] H. A. Ferwerda, J. Terpstra, and D. A. Wiersma, J. Chem. Phys. **91**, 3296 (1989).
[34] P. Cong, Y. J. Yan, H. Deuel, and J. Simon, J. Chem. Phys. **100**, 7855 (1994).
[35] J.-P. Foing, M. Joffre, J.-L. Oudar, and D. Hulin, J. Opt. Soc. Am. B **10**, 1143 (1993).
[36] K. Duppen, F. de Haan, E. T. J. Nibbering, and D. A. Wiersma, Phys. Rev. A **47**, 5120 (1993).
[37] N. Tang and R. L. Sutherland, J. Opt. Soc. Am. B **14**, 3412 (1997).
[38] C. H. Brito Cruz, J. P. Gordon, P. C. Becker, R. L. Fork, and C. V. Shank, IEEE J. Quantum Electron. **QE-24**, 261 (1988).
[39] W. T. Pollard, S. L. Dexheimer, Q. Wang, L. A. Peteanu, C. V. Shank, and R. A. Mathies, J. Phys. Chem. **96**, 6149 (1992).
[40] Y. J. Yan, L. E. Fread, and S. Mukamel, J. Phys. Chem. **93**, 8149 (1989).
[41] R. E. Walkup, J. A. Misewich, J. H. Glownia, and P. P. Sorokin, J. Chem. Phys. **94**, 3389 (1991).
[42] E. Tokunaga, A. Terasaki, and T. Kobayashi, J. Opt. Soc. Am. B **13**, 496 (1996).

[43] J. Chesnoy and A. Mokhtari, Phys. Rev. A **38**, 3566 (1988).
[44] J.-L. Oudar, IEEE J. Quantum Electron. **QE-19**, 713 (1983).
[45] *Handbook of Mathematical Functions*, edited by M. Abramowitz and I. A. Stegun (Dover, New York, 1972).
[46] R. W. Hellwarth, Prog. Quantum Electron. **5**, 1 (1977).
[47] T. Steffen, J. T. Fourkas, and K. Duppen, J. Chem. Phys. **105**, 7364 (1996).
[48] I. Kang, S. Smolorz, T. Krauss, and F. Wise, Phys. Rev. B **54**, R12 641 (1996).
[49] R. Hellwarth, J. Cherlow, and T-T. Yang, Phys. Rev. B **11**, 964 (1975).
[50] V. M. Farztdinov (private communication).
[51] Q. Hong, J. Durrant, G. Hastings, G. Porter, and D. R. Klug, Chem. Phys. Lett. **202**, 183 (1993).
[52] S. Ruhman, A. G. Joly, and K. A. Nelson, IEEE J. Quantum Electron. **QE-24**, 460 (1988).
[53] R. Merlin, Solid State Commun. **102**, 207 (1997).
[54] P. Simon, S. Szatmari, and F. P. Schäfer, Opt. Lett. **16**, 1569 (1991).
[55] P. McMillan, B. Piriou, and R. Couty, J. Chem. Phys. **81**, 4233 (1984).
[56] G. Herzberg, *Infrared and Raman Spectra of Polyatomic Molecules* (Van Nostrand Reinhold Co., New York, 1945).
[57] M. Cho, M. Du, N. F. Scherer, G. Fleming, and S. Mukamel, J. Chem. Phys. **99**, 2410 (1993).
[58] J. K. Ranka, R. W. Schrimer, and A. L. Gaeta, Phys. Rev. Lett. **77**, 3783 (1996).
[59] J. A. Walmsley and C. L. Tang, J. Chem. Phys. **92**, 1568 (1990).